

Article

Conceptual Navigation and Positioning Solution for the Upcoming Lunar Mining and Settlement Missions Based on the Earth's Mining Experiences: Lunar Regional Navigation Transceiver System

Danijela Ignjatović Stupar ^{1,*}, Vukan Ogrizović ², Janez Rošer ³, Vesna Poslončec-Petrić ⁴
and Goran Vižintin ³

¹ Department of Space Application, International Space University, 1rue Dominique Cassini, 67400 Illkirch-Graffenstaden, France

² Faculty of Civil Engineering Subotica, University of Novi Sad, Kozaračka 2A, 24000 Subotica, Serbia

³ Faculty of Natural Sciences and Engineering, University of Ljubljana, Aškerčeva cesta 12, 1000 Ljubljana, Slovenia

⁴ Faculty of Geodesy, University of Zagreb, Kačićeva 26, 10000 Zagreb, Croatia

* Correspondence: danijela.stupar@isunet.edu

Abstract: Precise drilling and excavation in future Lunar mining sites as well as in building habitats areas will be supported by robotized instrumentation. To ensure accurate positioning of facilities or structures, customized surveying instruments will be used to perform measurements needed for calculating locations of surveyed objects. Precise positioning in unexplored areas is difficult, even on the Earth, with all available support. This issue becomes even more complex on the Moon's surface, considering environmental conditions and the absence of Earth logistics. This paper solves a problem of centimeter-precision positioning on the Moon's surface. The solution is called Lunar Regional Navigation Transceiver System (LRNTS). It is based on a network of transceiver facilities, holding onboard both navigation transmitters and receivers. Transmitting modules of LRNTS act in the same way as the Global Navigation Satellite Systems (GNSS) space segment, sending navigation messages to the receivers. Receiving modules are needed for self-calibration of LRNTS to calculate their coordinates. In this paper, 12 different LRNTS-simulated configuration setups within Shackleton Crater are tested against positioning accuracy and visibility along the crater. The results show that LRNTS of nine transceivers can achieve sub-centimeter horizontal and better than 2 cm vertical accuracy, with consistent visibility of six and more transceivers throughout the Shackleton Crater.

Keywords: Lunar navigation; pseudolite; transceiver; control network; Shackleton Crater; Lunar mining



Citation: Ignjatović Stupar, D.; Ogrizović, V.; Rošer, J.; Poslončec-Petrić, V.; Vižintin, G. Conceptual Navigation and Positioning Solution for the Upcoming Lunar Mining and Settlement Missions Based on the Earth's Mining Experiences: Lunar Regional Navigation Transceiver System. *Minerals* **2023**, *13*, 371. <https://doi.org/10.3390/min13030371>

Academic Editor: Paul Alexandre

Received: 24 December 2022

Revised: 27 February 2023

Accepted: 4 March 2023

Published: 7 March 2023



Copyright: © 2023 by the authors. Licensee MDPI, Basel, Switzerland. This article is an open access article distributed under the terms and conditions of the Creative Commons Attribution (CC BY) license (<https://creativecommons.org/licenses/by/4.0/>).

1. Introduction

The drastic demand for natural resources has increased drastically in the last century. The reason for this is the large increase in population and rapid progress of green and nano technologies. Population growth also causes a much greater need for energy, food, and natural resources that disappear over time and are not renewed.

By switching to sustainable sources such as solar, wind, geothermal, and hydropower, urbanization and urban expansion can provide a light economic profit. However, due to the accelerated consumption of energy sources, climate change will be significantly highlighted, and thus we automatically reach unsustainability. Not long after, the amount of non-renewable natural energy sources, such as rare-earth elements (REE), precious and platinum group metals, and phosphorus and potassium, including fossil sources, will quickly be depleted with the increase in urbanization.

The political situation is also not on the positive side of the entire issue. The existing terrestrial resources, which are not evenly distributed throughout the planet, are treated

locally, not globally, which is against the establishment of World Trade Organization (WTO) regulations [1].

Due to the possession and use of rare natural resources, the countries of the Middle and Far East such as China, Russia, India, Saudi Arabia, etc., are advancing much faster economically compared to the United States and Europe. They own these resources and run the global economic market. There is also an awareness among the countries that their “precious and globally rare” energy sources will come to an end very soon. One of the reasons why they are also in the game is to find new sources that are beyond the borders of our planet. Investing in the research and exploration of new destinations in our solar system, where new energy sources will be exploited, represents a new era of competition between economically strong countries. This time, many more of them are in the race compared to the Cold War period when the Russians and the Americans were the only rivals.

In our solar system, there are three potential destinations where space resources can be pursued. The first targeted destination will be the Moon, where excavation technologies will be tested, followed by asteroid mining, and finally the planet Mars [2–4]. This paper is focused on the Lunar exploration scenario.

Nowadays, the Moon is experiencing newfound interest four decades after the termination of the Apollo program, with an objective to become a transfer station for exploration and settling outer space soon. It is the best test bed for In Situ Resource Utilization (ISRU) and application of new technologies in the production of consumable products such as water, propellant, and construction materials for the establishment of the first human life experiences on the Moon [5]. In the exploitation of Lunar resources and the settlement race, there are many programs currently ongoing, such as ARTEMIS, with worldwide partners involved. These include the ILRS (International Lunar Research Station) as a joint program between Russian Roscosmos and the Chinese CNSA national space agencies, together with the Chinese Chang’e program, and last but not least the Chandrayaan Program from the Indian Space Research Organization (ISRO) [2,6–10]. Different from the past, there are many other private companies interested in exploring the Moon and they do not necessarily come from the space sector. One of them is Rio Tinto, who plans to expand their currently used autonomous mining technology, such as automation, digitization, and advanced data analytics, in planetary mining [11,12]. For all of them, the main objectives are to find the best solution on how to excavate and use in situ Lunar resources to sustain life and work on the Moon for a long period of time.

The experience and importance gained in mining on Earth, in terms of technique, excavation methods, treatment, etc., will be transferred to the new circles of Lunar mining, with modifications according to the Lunar environmental conditions as well. Navigation and positioning, which play important roles in mining today, will also have a special importance in the connection between external and in-mine control networks [13].

In line with that, a Lunar navigation system is one of the requirements which must be taken seriously into account when missions coming from different programs occur together and when the construction of the habitats, launching pads, and the extractions from potential Lunar mining sites start. Various needs for a high-precision positioning and navigation system will arise in mining and civil engineering fields, such as to precisely calculate the quantity of extracted ore, to build infrastructure, and to superpose objects (e.g., on top of each other or nearby).

The problem of Lunar navigation is treated mostly in projects and papers investigating landing on the Moon’s surface and the navigation of robotized Lunar vehicles in limited areas. Accuracy demands for those applications are far from the mm or even cm level, but rather close to a few hundred meters [14]. Nevertheless, the suggested methodologies can be considered as a good starting point for designing the Lunar navigation network. Most of the suggested approaches apply and improve navigating concepts already known on the Earth, namely, inertial systems or navigating by image processing. None of those technologies can be applied as-is on the Lunar surface because of special instrumentation

requirements and specific environmental conditions. The huge difference between the Earth and the Moon, in the sense of gravity, atmosphere, temperature, humidity, etc., makes replication of classical Earth-related surveying methodologies very hard to implement on the Moon. This paper elaborates on the methodology of achieving cm-level accurate positioning in real time on the Moon, which is validated by presented numerical results.

2. Materials and Methods

2.1. Overview of Previous Research

Prior to further establishment of long-time robotic and human missions on the Moon, a consistent system for precise landing, navigation, and positioning is needed to accommodate continuous and safe work. At present, the navigation of objects located on the Lunar surface is controlled by Earth-based deep space network antennas [15]. Current investigation on navigation methodologies is based on technologies and working principles related to imaging, celestial (“star sensors”), inertial, and GNSS-like systems. They are introduced in following paragraphs.

There are several propositions based on imaging concepts using a camera as a navigating tool. Vision-based navigation is a technique suggested by major space agencies, aiming to achieve 200 m accurate autonomous landing [16]. So called pin-point Lunar landing uses an optical navigation system based on tracking features on the images by measuring an angular rate and a velocity vector of the spacecraft. Another possibility is to identify those features using a geo-referenced database to determine the position of the spacecraft. Using this technique, the position and velocity estimation accuracy of a spacecraft reaches approximately 10 m at 0.05 m/s. It was noticed that illumination conditions represent main issues for this optical Lunar navigation system [16].

For path planning and rover control, the successor of Yutu-1, Chang’e-4 Yutu-2 rover, used an upgraded version of an autonomous navigation system called visual Simultaneous Localization and Mapping (SLAM), which is based on tracking rover moves detected as a part of an image by a photogrammetric computer [17].

ESA, as a collaborative member on the Luna-27 mission, is developing the PILOT system as a main navigation system for the landers. The system compares the images of terrain landmarks taken by a camera and landmarks pre-stored in a database on the spacecraft to perform optical recognition of the crater’s landmarks for soft landing [18].

In the absence of satellite navigation systems, another navigation approach is possible, using star sensors supported by inclinometers. The Strapdown Inertial Navigation System (SINS) is a method based on a combination of two operational steps, approximate and fine navigation. The coarse positioning is used for initial alignment providing a real-time solution where all navigation errors were calculated and compensated in real time by SINS. Error corrections in SINS are done by the star sensors. Results from simulation have shown that this method can achieve high precision for rovers’ autonomous navigation [19,20].

For autonomous navigation, using only inertial navigation is not efficient due to growth of imperfections of inertial sensors which can provide relatively precise autonomy only for very short time. For that reason, a combination of inertial navigation with celestial navigation was suggested in [19,20].

The simulation presented in [19,21] applied the SINS method for the autonomous navigation of the rovers. In this model, starlight imaging was used, where the star sensor determines the altitude of the vehicle. The tilt angle between the horizontal plane and a vehicle is measured by a dual-axis inclinometer. Apart from the star sensor and inclinometer, attention was also paid to the utilization of precise clocks to provide real-time data and to synchronize data between two sub-segments of the compound navigation system. Misalignment of the star sensor and inclinometer can cause a significant positioning error. To avoid this systematic influence, the QUaternion ESTimator (QUEST) calibration method is introduced. This model can provide continuous measurements for only a few minutes, providing autonomous positioning accuracy from 20 m to 70 m in distance.

To support robotic missions, a constellation of the small satellites is considered as a technology that could resolve the navigation issue. It was suggested that the satellites might be placed into halo orbits in Earth–Moon libration points or LaGrange points [22,23].

An extension of the GLONASS navigation system is proposed in [24] to modify the satellites using additional narrow-beam antennas directed to the Moon. It would be implemented in the form of a constellation of six navigation satellites located in near-circular orbits at ~100,000 km height in two perpendicular planes with an inclination of 90°. Standard Satellite Navigation Equipment (SNE), a transmitter/receiver, and modified software for Moon usage would be integrated onboard a Lunar orbiting spacecraft and objects based on the Lunar surface. Simulation of this conceptual design has shown that position and velocity of the spacecraft can reach 15 m (1σ) in position and 0.02 m/s in velocity. For the objects based on the Lunar surface, it was highlighted that instantaneous navigation solutions can be provided only if the geodetic map with high precision is memorized in the SNE. Under this condition, if the objects are in the visible Lunar disk, the navigation accuracy is 10 m (1σ). While objects move away from the center, the accuracy degrades (e.g., for 60° deviations from the disk, errors can reach 20 m to 100 m). It was concluded that the proposed method cannot be used for navigating the objects on the far side of the Moon [24].

Yet another example is a GPS-based local area positioning system developed by the Aerospace Robotics Laboratory (ARL) at Stanford University for the planet Mars. The ground-located pseudosatellites replace the space-located satellite constellation with the goal of providing similar performance to GNSS on the Earth. Enabling localization is directed by a Self-Calibrating Pseudolite Array (SCPA). A network of transceivers is a way to expand the coverage of the system. The mathematical model of positioning the transceivers, which will both transmit and receive GNSS-like signals, used SCPA [25]. Field tests were performed using a prototype of NASA Aims K-9 Mars rover achieving code- and carrier-level positioning less than 3.7 m and 8.8 cm, respectively [26,27].

In the case of open-pit mining, ARL at Stanford University developed a guidance system for transport and operational vehicles based on pseudo-assisted Carrier-Phase Differential GPS. With this system, a narrow angle of open sky above the pit and a small number of visible satellites will be mitigated by six or eight pseudolites placed around the rim. This system will augment the existing GPS constellation and ensure the availability of navigation anywhere inside the pit [27,28].

NASA envisaged the Artemis program to develop a special receiver which will be able to receive signals from the Global Positioning System (GPS). This receiver is based on the same working principles as receivers used for high-altitude navigation in Magnetospheric Multiscale mission (MMS) and Geostationary Operational Environmental Satellites (GOES) in combination with the GPS processing power of NavCube receivers [29].

To this day, there is no satellite navigation system which will help spacecraft to be navigated autonomously to the Moon. This is only supported by constant controlling from the Earth, which will be extremely complicated when multiple missions are shuttling and maneuvering backwards and forwards.

Dozens of missions to the Moon are planned and some of them already started, with initial executions such as NASA's Artemis 1 and ispace's HAKUTO-R Missions 1 [30,31].

Experiences gained via the Artemis 1 mission, where the capabilities of the Orion's systems were tested, showed that loss of communication with spacecraft can happen easily at the moment when the vehicle is located behind the Moon. Moving through space, the Earth is the only point of reference when a returning ping signal will provide the position of the spacecraft. If there is an obstacle between them, there will be plenty of blind spots and high risk of a complete loss of communication. To solve this problem, there is need for triangulation from an autonomous navigation system. NASA and ESA are working on the development of the Lunar navigation network, which will be the main system helping all upcoming Lunar missions [32].

The Moonlight Initiative ESA's program includes a series of missions which will maintain sustainable Lunar exploration. A part of the mission is the establishment of a navigation constellation of three to four Lunar Pathfinder satellites orbiting the Moon in Elliptical Lunar Frozen Orbit (ELFO), mainly covering the Lunar South Pole [18]. Launch is planned for a period between 2025 and 2026. The mission objective is to demonstrate high-bandwidth communication and navigation capabilities for the future Lunar missions. The Lunar Pathfinder will also support the Lunar Polar Sample Return mission, which aims to retrieve samples from the Moon's South Pole region. A mission developed by ESA and the satellites built by Surrey Satellite Technology LTD (SSTL) will have a NaviMoon receiver onboard [4]. The receiver's capacity will be to harness the navigation signals (strong and weak as well) from the terrestrial navigation systems (GPS and Galileo), determining the Pathfinder position with approximately 60 m accuracy. The Lunar lander Argonaut, as a part of the Moonlight Initiative mission together with the Pathfinder satellites, will help the rovers in positioning on the Lunar surface [32].

The Lunar GNSS Receiver Experiment (LuGRE) is developed in partnership between NASA and the Italian Space Agency (ASI) based on laser retroreflector technology. Mirrors on the Pathfinder's array will aim to enhance Lunar navigation and to validate operational capabilities, which will also be critical for Artemis and the future missions [33].

The review of many proposals, simulation models, and feedback from landers' and rovers' experiences can be summarized in a general conclusion that all of them are based on autonomous navigation without the possibility to connect and to collaborate under the same system. The model proposed in this paper is based on pseudolite transceiver field tests introduced by ARL from Stanford University and applied for open-pit mining and for a Mars navigation system. With a similar Moon scenario in the Shackleton Crater, our stand-alone navigation system will serve all users from the same Lunar region. In the next stage of development, when the Pathfinder constellation from the Moonlight Initiative program is operational, it will be used for referencing all local coordinates obtained by the system elaborated in this article to the Lunar reference system.

2.2. Study Area

Several environmental and technical factors influence the choice of navigation methodology: temperature, illumination, communication with Earth, and Lunar topography. The Moon's position in the solar system and its relationship with the Earth and the Sun open an important topic on the selection of regions for future settlement. Therefore, the area around the South Pole is the most attractive location for Lunar exploitation [34]. The orientation of the Moon's rotation axis, which is tilted 1.5° from the ecliptic plane, makes the Lunar poles mainly Permanently Shadowed Regions (PSRs), meaning that the floors of some craters from these regions never receive sunlight. Consequently, the temperature in these characteristic craters allows the sustainability of Lunar ice. This confirms a hypothesis based on evidence of the potential existence of water on the Moon, thus guaranteeing the possibility of living and working on the Moon [35]. However, regions which never receive direct solar illumination still receive sunlight coming to them indirectly, scattered, with the addition of starlight. This issue is elaborated in several statistics on measured quantities of solar power supply in all regions, including the polar ones [36–38].

Important conclusions on the South Pole area are drawn from results of processing topographical, geological, and environmental datasets collected by diverse Lunar missions (Apollo, Luna, Molnya, Chandrayaan, Chang'e, Lunar Reconnaissance Orbiter (LRO), Clementine [36,39], SELENE [40], etc.), making this area the best candidate for permanent Lunar settlement. Figure 1 introduces the polar-based region, where high attention is given to Shackleton Crater, located inside the rim of the South Pole Aitken (SPA) Basin [36,39,41,42].

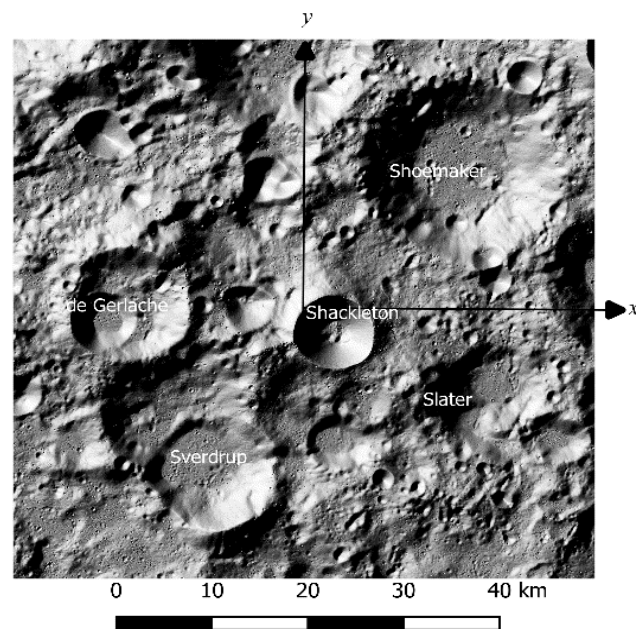


Figure 1. Lunar South Pole.

Furthermore, communication with the Earth plays an important role in site selections. That is why the potential sites in the South Pole region based near the Shackleton Crater rim and Mons Malapert crater fulfill the requested parameters. They are noted as the best areas for a relay station due to high altitude, topographic characteristics, and visibility with the Earth [43]. In the case of simultaneous establishment of the laser relay on the North Pole, communication with the Earth will be 100% covered. Two separate systems per pole with 100 km distance between them will enable robust local wireless communication coverage [36].

Concluding on the selection of the study area for this research, the analysis of the discussion on the Moon's South Pole region characteristics showed that Shackleton Crater fulfills all technical and environmental requirements. Therefore, simulation and statistical analysis of positioning accuracy will be carried out using Shackleton Crater as a case study. The presented methodology is replicable to other regions as well as other celestial bodies.

2.3. LRNTS Configuration

In Earth-based surveying, for each site, a control network is developed prior to further positioning works. The control network is designed in such a way as to spread over the whole site to avoid any extrapolation coming from a coordinate frame definition, which could jeopardize positioning accuracy. It is implemented as a set of stable, fixed points or facilities. Characteristic points of objects that are to be placed at the site are connected to the control network points with relative measurements, such as distances, angles, or coordinate differences. Consequently, both control networks and objects' points' coordinates share the same coordinate system.

The core of this research is developing a methodology that will allow real-time centimeter positioning accuracy throughout large areas of the Moon's surface. The targeted accuracy should be:

- available in real-time;
- homogeneous throughout the whole area of interest;
- independent of the size or the shape of a construction/exploration site;
- replicable elsewhere (other solar system bodies).

A solution presented in this paper suggests placing a set of transceivers along the crater rim, forming a system that would act like any GNSS cosmic segment. LRNTS distinctions from GNSS are summarized in three items:

- LRNTS is a ground-based system;
- it consists of transceivers instead of transmitters;
- it is self-adjustable.

LRNTS is implemented as a coordinate frame materialized by a set of transceivers located along a crater rim. Each transceiver acts, at the same time, as a transmitter and a receiver. As the transmitter, it broadcasts GNSS-compatible signals to other transceivers (and also inside the crater), while, as the receiver, it receives navigation messages from other transceivers. In that way, LRNTS can adjust the crater coordinate frame only by mutual measurements between LRNTS sites, unless tight fitting into the Moon reference system is needed. Self-calibration of LRNTS is performed via an iterative adjustment of measurements acquired mutually between the LRNTS nodes. One of the tested configurations analyzed in this paper, which is elaborated in detail later, is schematically represented in Figure 2. Blue dots represent LRNTS nodes, while black lines indicate established connections between the nodes. The intention is to provide as much visibility as possible between the transceivers. However, due to crater topography, not all baselines could be established.

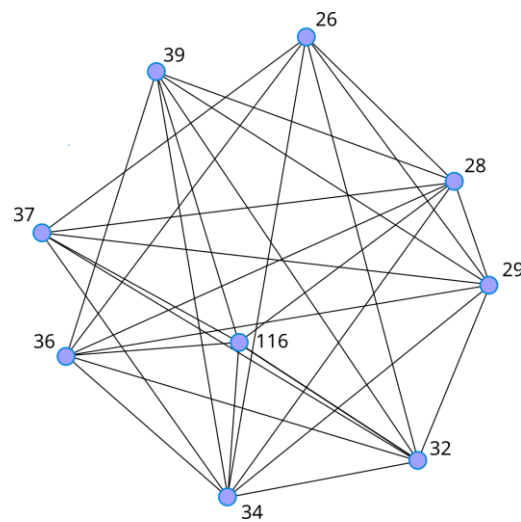


Figure 2. A scheme of interconnection between LRNTS sites.

Following the Lunar surface exploration objectives elaborated in [44], LRNTS is designed to act as a foundation positioning tool for all human and robotic missions in phases 1–3 of the Lunar surface exploration operation concept. The behavior of equipment exposed to harsh Lunar conditions can be tested against real conditions in three different environments: controlled indoor lab, virtual simulation, or outdoor analogue testing [45]. The operation of LRNTS transceivers will follow recommendations from [46], stated for robotic missions supporting the installation and maintenance of a permanent human Lunar base. Since solar power is seen as the most appropriate power source for Moon applications, microgrids can be used for powering all the facilities and vehicles in an area of interest [47].

The navigation system presented in this paper represents a solution for extra-terrestrial positioning applications where there are no satellite navigation systems available yet. Specially, because of existing data for the Moon topography, its explorations so far, and current interests for its further utilization, this paper suggests a pseudosatellite-based regional Lunar navigation system, which makes positioning activities on the Lunar surface much more precise. In addition to that, it is economic and self-sustainable, with no need for real-time monitoring.

2.4. A Coordinate System, a Map Projection, and a Timeframe

The LRNTS coordinate frame is based on 10 m Lunar Digital Elevation Model (DEM) [48]. If a more precise and detailed Moon reference frame would be introduced in the future, the LRNTS coordinate frame (and all sites within the crater tied to it) would be easily

transformed into the new system. Throughout this study case, the LRNTS frame is treated separately from any Lunar reference system. Any such connection would introduce error sources related to global reference frame definition and implementation, which would create a false result on LRNTS performance. If this methodology proves its hypotheses and if other environments like Shackleton are to be investigated, then a tie to a Lunar reference system would be implemented. A possible solution for implementing a Lunar frame would be five Lunar Laser Ranging (LLR) retroreflectors, already placed on the Lunar surface. Their positions are determined with a cm level of accuracy, which makes them a good candidate for the reference frame implementation. Their coordinates are expressed as Cartesian 3D X, Y, Z coordinates, with the coordinate system origin in the Moon's center of mass, with no projection defined. Furthermore, where appropriate, spherical latitude–longitude–height coordinates can be used [49,50].

Although very simple, Cartesian X, Y, Z coordinates with an origin at the Moon's center of mass are not convenient for practical large-scale and precise applications. Therefore, we suggest here a polar xy stereographic projection, with the origin at the Moon's South Pole, as depicted in Figure 1. All simulated measurements and calculations in this study are done in the polar xy stereographic projection.

The LRNTS timeframe is based on the transceivers' atomic clocks. Each transceiver node holds an Atomic Frequency Standard (AFS) onboard (Figure 3), thus providing the same time reference for both transmitting and receiving segments. The benefit of this approach is that clock correction terms coming from different time standards (as with GNSS, for example) are neglected in measurement equations since transmitters and receivers use the same time system. A joint LRNTS timescale is developed from all LRNTS clocks, distributing time system parameters to each transceiver. Performance of one-way GNSS timing is estimated to about 20 ns [51], where a significant share in the error budget is related to ionospheric and tropospheric delays. LRNTS timeframe stability is expected to be better for an order of quantity than GNSS, having in mind theoretical one-way transfer accuracy of 100 ps for code ranges and 1 ps for carrier phase measurements [52]. However, the stability of LRNTS clocks should be checked on regular basis by time series analysis of LRNTS daily solutions (transceivers coordinates).

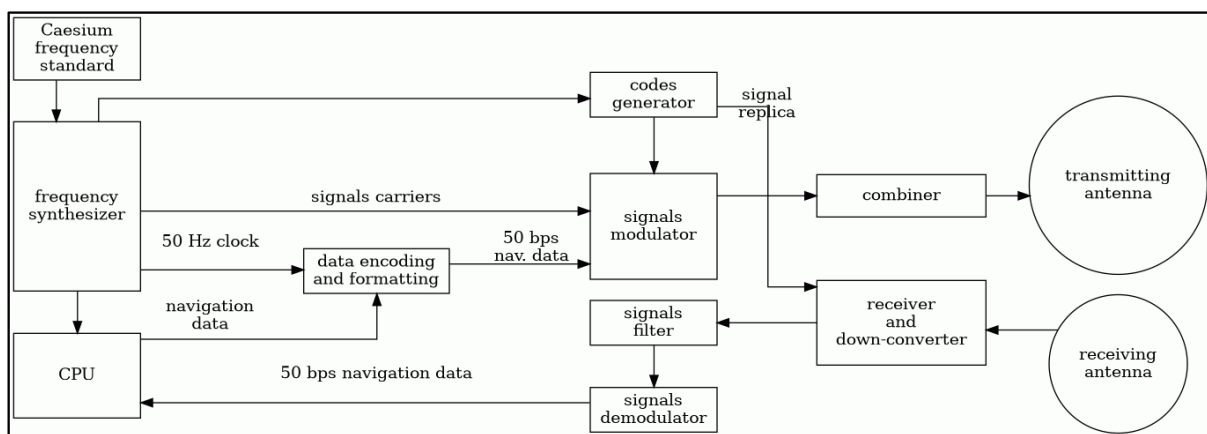


Figure 3. Conceptual diagram of a transceiver.

Furthermore, differences in gravity conditions between the Moon and Earth have an impact on the operation of atomic clocks. The differences in gravitational potential between the Moon and Earth can cause a change in the resonant frequency of the atoms, which is known as a gravitational redshift. This redshift can result in a shift in the frequency of the atomic clock, leading to inaccuracies in time measurements. Furthermore, the effects of special and general relativity also need to be considered. Special relativity affects the ticking rate of clocks, whereas general relativity causes a change in the geometry of space-time. Finally, thermal effects are important for precise definition of the Lunar timescale,

resulting from rather different temperature conditions on the Moon compared to Earth. Changes in temperature can cause changes in the resonant frequency of the atoms, leading to inaccuracies in time measurements. To mitigate these effects, atomic clocks must be designed and tested to withstand the harsh conditions on the Moon and to account for the effects of different gravity conditions. Since the Lunar timescale is developed from measurements from all transceivers, special error correction algorithms are implemented to improve the accuracy of time measurements.

When the Pathfinder constellation is completed, LRNTS transceivers would be able to collect measurements from the Pathfinder satellites and, thus, to calculate their coordinates in the Lunar reference frame. Here it is assumed that the Pathfinder satellites' coordinate frame will correspond to the Lunar reference frame. Then, transformation parameters from the local LRNTS system to the Lunar reference would be calculated using some Affine transformation models. Implementing the transformation parameters, all local coordinates could be transformed to the Lunar reference frame. LRNTS improves the concept [26] in a way that it will be used as a static transmitter constellation. After its establishment and self-calibration, when all LRNTS nodes obtain their coordinates, its role will be like any GNSS cosmic segment, providing navigation messages to the receivers performing regular surveying tasks within the crater.

3. Results

3.1. Transceiver Concept

A transceiver, in the LRNTS sense, is a system capable both of transmitting and receiving navigation messages. Basically, it would be implemented as a compound device, consisting of:

- a pseudolite generating GNSS navigation messages, which are transmitted via a transmitting antenna;
- a GNSS receiver, which receives the signals sent by other transceivers in the network.

A conceptual diagram of such a transceiver node is given in Figure 3. Some functions are shared between the transmitter and receiver: AFS, frequency synthesizer, and CPU.

The transceivers transmit and receive the signals at the same frequencies simultaneously. Therefore, interference between transmitted and received signals is likely to occur. This issue, called a near-far problem, is already recognized in terrestrial navigation applications, where augmentation of GNSS signals is needed, for example, in aircraft landing. Weak GNSS signals receive interference from strong pseudolite signals, which can completely block reception of the navigation messages by the GNSS receivers at the aircraft. Interfering signals can be processed in the transmitting and receiving phase. A latter approach is implemented, for example, in Successive Interference Calculation (SIC). This method reduces the effects of received signals with power above the ambient noise [53]. Antenna diagram shaping could help in reducing the near-far effect, which is summarized in [54]. A mitigation scheme combining two methods, Frequency Domain Excitation and Direct Reconstruction Cancellation, is used for solving for both continuous-wave and pseudolite-type interferences [55]. Narrowband interference can effectively be mitigated by temporal filtering methods, especially when the time domain and space domain methods are integrated. Such an antenna array Space Time Processing (STP) approach is elaborated in [56].

Interference between the transmitted and received signals in an LRNTS transceiver that operates in full duplex mode can be solved by using time-division multiplexing (TDM) or frequency-division multiplexing (FDM). In TDM, the transceiver alternates between transmitting and receiving at different times, effectively separating the transmitted and received signals in time. In FDM, the transceiver uses different frequencies for transmission and reception, avoiding the overlap of the signals.

Furthermore, advanced filtering techniques can be used for minimizing interference between transmitted and received signals, for example, the usage of band-pass filters or notch filters, which eventually remove the transmitted signal from the received one.

Additionally, using directional antennas can also reduce the amount of interference by limiting the amount of transmitted signal that reaches the receiver.

The decision of where exactly to land the transceiver depends on the local terrain configuration. As stated before, the approximate locations for the transceivers were determined by examination of the 10 m DEM. The landing spot, which should be horizontal and with no significant obstacles nearby, can be selected using various landing techniques, for example, a multi-model hierarchical scene matching model [57] or an indirect scheme based on a two-point boundary value problem [58]. A method for obstacle detection during landing is elaborated in [59]. The sensitivity of the transceiver node's location does not influence the stability of the LRNTS mathematical model, which is statistically proven in latter subchapters. It means that the transceiver can be landed anywhere within a few tens of meters around the preliminary location if the spot is horizontal and without significant obstacles.

The mathematical model of positioning using LRNTS, introduced in latter subchapters, assumes that both transmitting and receiving antennas of the transceiver refer to the same phase center, which is, generally, not the case. Therefore, the relative relationship between them should be determined during the calibration process, which is performed before sending the transceiver towards the Moon. The calibration of the mutual spatial relationship between the transmitting and receiving antennas is not included in further calculations. For the rest of this research, while not jeopardizing the reliability of the conclusions, it will be assumed that both antennas share the same phase center.

The multipath effect is a part of the positioning error budget. It depends on the terrain configuration and physical properties of the environment. The analysis of detailed Shackleton topography and the physical characteristics of regolith is beyond the scope of this paper. It can be assumed that multipath will not be a critical factor for accuracy degradation, since the average Bond albedo of the Moon is 0.11, but further research on this issue will give more precise conclusions. The application of Lunar surface reflectance models [60] or [61] can be used for preparing detailed multipath models of the Shackleton Crater.

All measurements from all transceiver nodes are sent in real-time to a master station, where processing is performed. Final coordinates are sent back to each transceiver. The master station is the transceiver at the location visible from all other nodes.

When the system is calibrated and fully operational, it operates as a GNSS space segment, sending navigation messages to LRNTS receivers. Then, the requirements for user LRNTS receivers can be similar to classical GNSS receivers, including the usage of crystal clocks.

3.2. Challenges of Lunar Environmental Conditions

The negative influence of the Lunar environment on hardware survival must be taken into consideration, especially for a long-duration mission. Analyzing previous mission experiences from the Luna and Apollo Programs, there are two major impacts underlined on hardware systems: Lunar regolith and sunless cold temperatures. Regolith comprises dust-sized particles between 40 μm and 130 μm and is extremely abrasive due to its chemical and physical composition [62,63]. Additionally, the Moon is permanently exposed to solar radiation and cosmic ray spallation, which makes constant contact with the regolith. Due to that phenomenon, particles are electrostatically charged, which represents a significant impact on the hardware. To mitigate Lunar dust influence on the hardware and Lunar operation, compliant mechanisms led by analytical design and topology optimization are proposed by [64,65].

Bearing in mind that solar energy will be unavailable during the lunar nights, this makes the production of heat and electricity challenging [63]. To avoid this problem, two solutions are proposed: (1) Thermal Wadis as a thermal power source to protect the systems during the cold periods and (2) Thermal Energy Storage (TES) as a system to run a heat engine producing the electricity during the periods of darkness [66].

Another problem of deploying instrumentation on the Moon's surface is related to harsh conditions on the Lunar surface, with daily temperature variations of almost 300 K. However, due to regolith's low thermal conductivity, the temperature under the surface remains almost constant, with an average of about 253 K [67]. Therefore, a possible solution for the long-term operation of a transceiver node is keeping its sensitive electronics under the surface while exposing only the necessary devices (antennas, motors, solar collectors, etc.) to the environment.

As a summary on operational consequences resulting from the specific Lunar environment, several issues are critical to keep sensitive electronic components operational. The first is related to thermal management. Electronic components must be able to withstand large temperature fluctuations and high temperatures. To mitigate this, insulation and thermal control materials, such as multilayer insulation (MLI) or thermal blankets, can be used to regulate the temperature of the electronic components.

The Lunar surface is subject to high levels of solar and cosmic radiation that can cause Single Event Upsets (SEUs) and Single Event Latchups (SELs) in electronic components. To mitigate this, various techniques such as using radiation-hardened components, shielding, and redundant systems are used.

Electronic components must also be mechanically protected from mechanical impacts and vibrations that can occur during landing and operation on the Lunar surface. This can be achieved using ruggedized packaging, shock mounts, and shock absorbers.

To ensure the longevity and reliability of electronic components, it is important to manage the power supply effectively. This can be achieved using power storage systems, such as batteries or energy harvesters, and power management systems that regulate the power supply to the electronic components.

3.3. LRNTS Observables

LRNTS observables are code pseudoranges and carrier phases, the same as with any GNSS. Regarding different Lunar conditions (geometric and environmental) compared to Earth GNSS, standard GNSS observable equations change in some terms.

A simplified form of a code pseudorange between two transceivers can be expressed as:

$$P = c(T_r - T_s) = c\Delta T \quad (1)$$

where T_r and T_s are signal reception and signal emission times, respectively, while c stands for the speed of light in a vacuum. Readings of the times T_r and T_s correspond to the receiving (r) and transmitting (s) transceiver, which yields:

$$P = c[(t_r + \delta_r) - (t_s + \delta_s)] = c\Delta t + c\Delta\delta = \rho + c\Delta\delta \quad (2)$$

With:

- t_r, t_s —readings of the received and transmitted signals, respectively;
- δ_r, δ_s —biases of the receiver and the transmitter clocks, respectively;
- ρ —the geometric distance between transceivers s and r .

The biases δ_r, δ_s are calculated per transceiver and are available via a navigation message. The complete pseudorange equation introduces other error sources:

$$P = \rho + c\Delta\delta + D_r + D_s + M_{rs} + \epsilon_{rs} \quad (3)$$

where:

- D_r, D_s —hardware delays for the receiver r and the transmitter s , respectively;
- M_{rs} —multipath term between r and s ;
- ϵ_{rs} —remaining random error of the measured pseudorange.

If a signal is transmitted at the frequency f , then the basic carrier phase equation is written as:

$$\Delta\varphi_{rs} = \varphi_r - \varphi_s = -f\frac{\rho}{c} - f\Delta\delta \tag{4}$$

where φ_s is the phase angle of the sent signal and φ_r is the received phase angle of the same signal. The carrier phase $\Delta\varphi_{rs}$ is expressed in cycles, taking values within one cycle, i.e., $[0, 2\pi]$. In order to measure the cumulative phase angle $\Delta\Phi_{rs}$, the number of whole cycles, known as the integer ambiguity N_0 , is involved. If the frequency f is expressed as a function of c and signal wavelength λ using the relation $f = \frac{c}{\lambda}$, the standard form of the carrier phase equation becomes:

$$\Delta\Phi_{rs} = -\Delta\varphi_{rs} = \frac{\rho}{\lambda} + \frac{c}{\lambda}\Delta\delta + N_0 \tag{5}$$

Elements of (5) are expressed in meters by multiplying it by λ :

$$\lambda\Delta\Phi_{rs} = -\Delta\varphi_{rs} = \rho + c\Delta\delta + \lambda N_0 \tag{6}$$

The final form of the carrier phase measurements also contains hardware delays (D_r), multipath (D_s), and a random measurement error (ϵ_{rs}), yielding:

$$\lambda\Delta\Phi_{rs} = \rho + c\Delta\delta + \lambda N_0 + D_r + D_s + M_{rs} + \epsilon_{rs} \tag{7}$$

N_0 corresponds to the number of full cycles in the first epoch. It is unknown, as in the case of GNSS. However, because LRNTS transceivers are static, the number of full cycles for a pair (transmitter, static receiver) does not change in time and can be determined after the second measuring epoch, because $N_0 = N_1 = N_2 = \dots$

3.4. LRNTS Self-Calibration Model

There are k transceivers in an LRNTS configuration setup, and they are distributed along the crater. Their approximate coordinates $T_i(X, Y, Z)_0, i = 1, 2, \dots, k$ are obtained from [48]. All transceivers are mutually connected with code ranges and carrier phase measurements:

$$P_{ij} = \sqrt{(X_i - X_j)^2 + (Y_i - Y_j)^2 + (Z_i - Z_j)^2} \tag{8}$$

$$\Delta\varphi_{ij} = \text{MOD} \left(\frac{\sqrt{(X_i - X_j)^2 + (Y_i - Y_j)^2 + (Z_i - Z_j)^2}}{\lambda}, 2\pi \right) \tag{9}$$

where $i, j = 1, 2, \dots, n$. The total number of independent measurements per epoch is, therefore,

$n = k \cdot (k - 1)$, while the number of unknown transceiver coordinates is $u = 3k$. Since all measurements are uncorrelated, the weight matrix \mathbf{P} is diagonal, with the elements $p_i = (\sigma_i^2)^{-1}$, where σ_i^2 is the measurement dispersion. The design matrix \mathbf{A} is a Jacobian with elements $a_{qm} = \frac{\partial O_{ij}}{\partial C_m}$, where O_{ij} is the observation function (8) or (9), and C_m is an unknown coordinate.

Index $q = 1, 2, \dots, n$ indicates a measurement, while $i, j, m = 1, 2, \dots, u$ are related to the unknowns.

The adjustment model used here is developed as a free 3D network. Therefore, the normal equation matrix $\mathbf{N} = \mathbf{A}^T\mathbf{P}\mathbf{A}$ is singular, so Moore–Penrose pseudoinversion is used for calculating a cofactor matrix $\mathbf{Q}_x = \mathbf{N}^+$. Coordinate increments are calculated as: $\mathbf{x} = \mathbf{Q}_x\mathbf{A}^T\mathbf{P}\mathbf{l}$, where \mathbf{l} is the vector of the measurements. After calculating the new coordinate values $\mathbf{X} = \mathbf{X}_0 + \mathbf{x}$, an iterative adjustment procedure is repeated, with coordinates

X from the previous iteration assigned as approximate ones for the next epoch. Standard deviations of the unknown parameters are calculated as:

$$\hat{\sigma}_{ii} = \hat{\sigma}_0 \sqrt{Q_{ii}} \tag{10}$$

With:

- $\hat{\sigma}_0 = \sqrt{\frac{\mathbf{v}^T \mathbf{P} \mathbf{v}}{n-u}}$ —a posteriori dispersion factor, where vector of measurement increments $\mathbf{v} = \mathbf{A}\mathbf{x} - \mathbf{l}$;
- Q_{ii} —corresponding element of the cofactor matrix \mathbf{Q}_x .

Self-calibration is a process that establishes but also regularly checks the LRNTS coordinate system. The measurements needed for self-calibration can be completed in a short time (in 1–2 min), due to the ease of solving the integer ambiguities, as stated earlier. Therefore, periodical checks of the coordinate frame may be performed on a monthly or even weekly basis. During the periodical checks, the system still broadcasts navigation messages, so the users do not need to pause their work.

3.5. Simulated Configuration Setups

Analysis and results in this research are performed on the Shackleton Crater; thus, DEM [48] is trimmed to match the area of interest. To simulate various LRNTS configuration setups, a number of points are digitized over the Shackleton DEM in order to obtain their 3D approximate positions. The points locations are not directed by any special rule, but rather spread around the crater. In Figure 4, the Shackleton Crater DEM is represented both as a false-color palette and a 300 m equidistance contour map overlapped with the possible locations of LRNTS transceiver nodes (marked as white triangles with their locally assigned IDs).

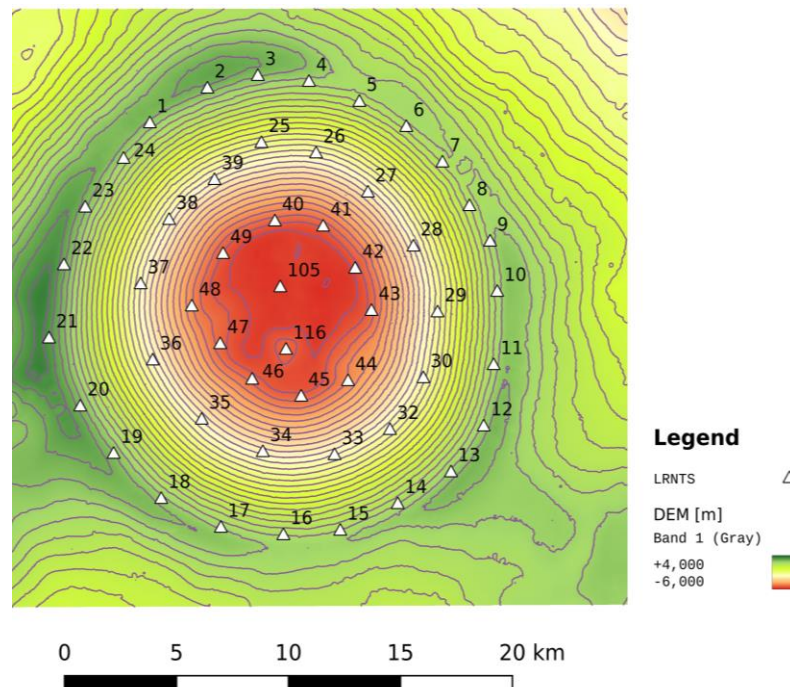


Figure 4. Candidate places for LRNTS transceivers.

The optimization of LRNTS treats locations and number of transceivers that would assure the best positioning performance within the crater. The optimal configuration of the LRNTS network should provide:

- enough measurands (i.e., number of transceiver nodes) for self-calibration of the system;
- signal coverage throughout (or, if not possible, for the majority of) the crater’s interior;

- reliable signal transmission by minimizing multipath effects.

The locations of the transceivers should allow the undisturbed mutual transmitting and receiving of navigation messages between all transceivers. The same goes for spreading the signals towards the crater bottom, where the surveying of construction sites will be done. The signals with lower elevation angles (closer to the ground) can experience multipath effects, since the transceivers are placed on the ground, not in space. Further analysis of Shackleton topography is performed by creating a slope map. The frequency histogram (Figure 5) of the Shackleton slope map shows that the majority of the crater is at cca 50° slope, which should be taken into account for future LRNTS utilization plans in order to avoid possible multipath effects during the transmission of transceivers' signals. The histogram values in Figure 5 are expressed in pixels.

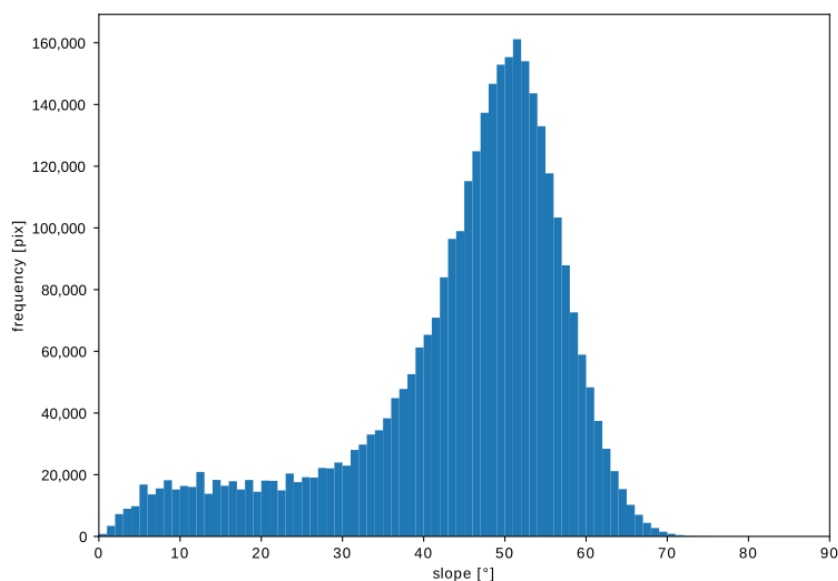


Figure 5. Histogram of frequencies for a developed slope map of the Shackleton Crater.

In addition to the careful planning of LRNTS transceivers' distribution in the sense of accuracy, the number and location of the transceivers should be optimized for the availability of the signals as well. Assuming future use of GNSS receivers for in-crater positioning, permanent visibility of at least four transceivers must be assured. Furthermore, for economic reasons, the total number of the transceiver nodes should be minimized.

Although a receiver can solve its position by collecting observations from only four satellites, experiences from terrestrial GNSS positioning show that, in realistic scenarios, it is not enough because of temporal obstacles that violate visibility of the sky. In the case of ground-based transceivers, that problem could arise as well. In addition, there is a practical maximum of the number of satellites where there is no significant increase in accuracy or reliability. Therefore, the selection of the number of transceivers per configuration and their locations is carried out by examining user experiences in terrestrial GNSS positioning.

First simulations involve 24 different configurations, from 5 to 24 transceivers. As stated before, the only criterion for choosing locations for the transceivers was their approximate uniform distribution along the crater. The positioning by four transceivers could be violated in the case of obstacles or a poor configuration. Therefore, we put 5 as a minimum for the number of LRNTS transceivers and 24 as a maximum, although the maximal number of the transceivers is theoretically not limited. However, increasing the number of LRNTS transceivers does not increase accuracy and reliability linearly. We have randomly chosen 33 different configurations. Among them, 12 are presented in this paper. Others are rejected because of their bad numerical figures.

The setups involve between 6 and 11 LRNTS transceivers. Individual setups with spatial allocation of the transceivers can be reviewed from Figure 6. Lines indicate intervisi-

bility between certain LRNTS transceivers. Only vectors between intervisible transceivers were included in the adjustment models.

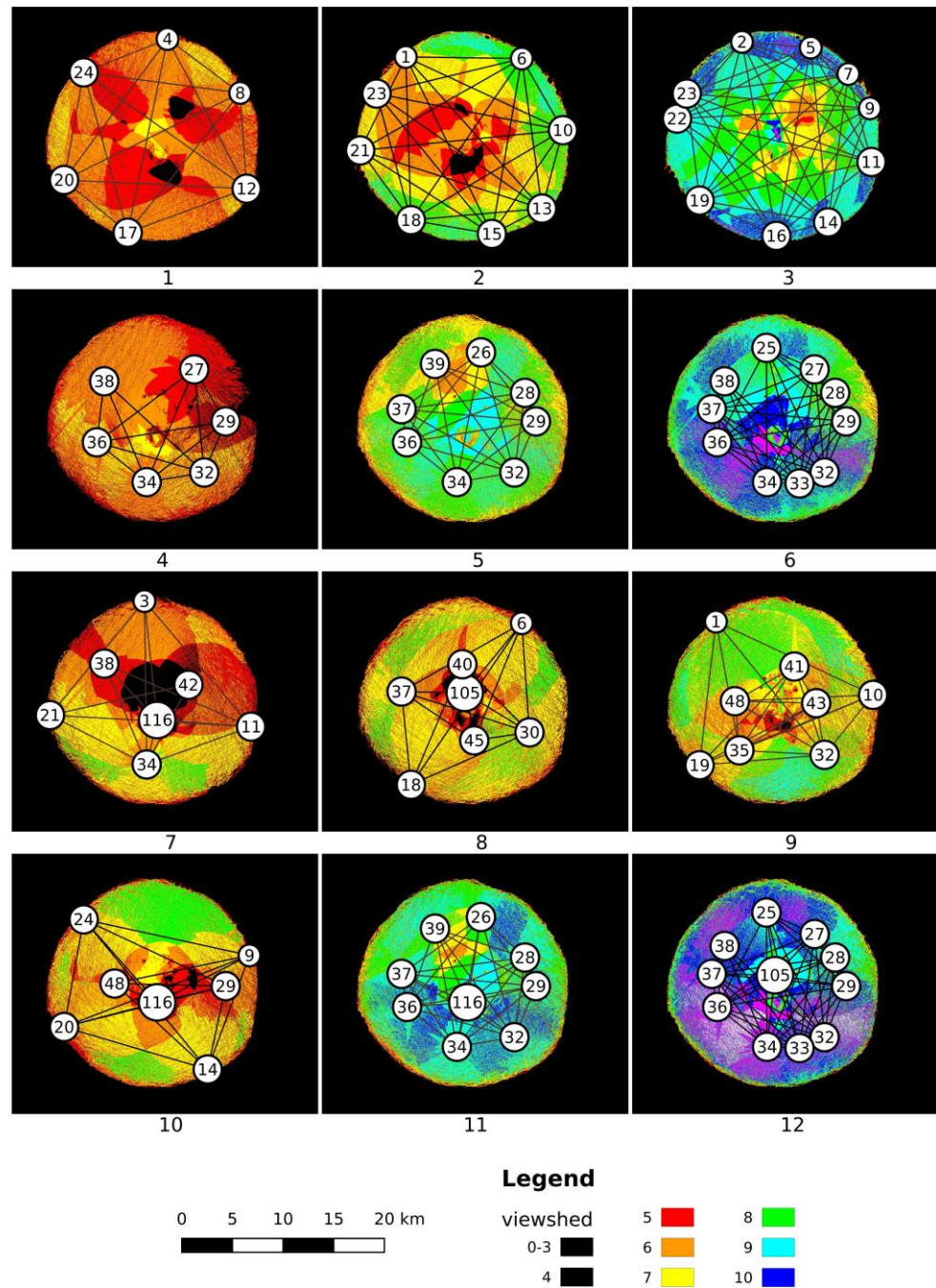


Figure 6. Viewsheds of transceiver signals.

For each configuration setup, a corresponding viewshed map is created, depicting the availability of LRNTS signals within the crater area, as shown in Table 1. In Figure 6, all maps 1–12 share the same color ramp, where each color represents a certain number of visible transceivers at the given point. All pixels with values below 4 are painted in black, suggesting that in those areas, LRNTS navigation is not possible due to the lack of the minimal number of visible transceivers. The locations of transceivers are marked as white circles, with the point ID within the circles. A quick review of the viewshed maps

indicates that the setups with more transceivers also imply better visibility on the surface of the bottom of the crater.

Table 1. LRNTS configuration setups.

Map Model No.	Number of Points	Number of Measurements	Number of Unknowns	% of Signal Availability
1	6	58	18	91.6
2	8	102	24	95.7
3	10	162	30	98.6
4	6	52	18	84.0
5	8	102	24	95.3
6	10	152	30	96.3
7	7	48	21	78.4
8	7	60	21	86.8
9	8	82	24	92.8
10	7	64	21	91.2
11	9	134	27	95.5
12	11	188	33	96.4

3.6. Self-Calibration

The self-calibration of LRNTS is performed as an iterative adjustment using the model elaborated in Section 3.3. Input parameters, in the sense of a priori quality characteristics and accuracy, are chosen by adapting standard error budget for GNSS positioning [68], adopting 300 cm for coarse-code code range accuracy and 5 mm for phase ranges. Multipath and atmospheric influences are neglected here. In addition, receiver clock bias is not treated in this study, because it refers to receiver crystal clocks, while all LRNTS transceivers hold atomic clocks aboard and use the same timescale for transmitting and receiving. The adjustment was performed adopting a 100 m spatial error of approximate LRNTS transceiver positions, resulting from DEM. The adjustment process converged after the third iteration in all tested models.

Table 2 summarizes the obtained results for all 12 tested models. Columns 2 to 7 contain minimum and maximum standard deviations of the points' spatial (3D), horizontal (2D), and vertical (1D) positions, respectively, which is further used for analyzing performance of the network geometry.

Table 2. LRNTS positioning performance depending on the model.

Map Model	(3D) σ_{xyz} (Min)	(3D) σ_{xyz} (Max)	(2D) σ_{xy} (Min)	(2D) σ_{xy} (Max)	(1D) σ_z (Min)	(1D) σ_z (Max)
(N°)	(mm)	(mm)	(mm)	(mm)	(mm)	(mm)
1	20.1	38.0	3.9	7.4	19.7	37.4
2	17.1	44.0	3.5	7.2	16.6	43.4
3	22.1	41.3	3.6	6.5	21.8	40.8
4	41.3	283.3	15.7	151.1	38.2	239.6
5	22.9	50.6	8.4	20.5	21.0	46.3
6	24.1	332.5	11.6	167	19.0	287.5
7	7.7	28.7	5.0	18.0	4.6	22.4
8	7.0	17.5	5.0	10.3	4.9	15.0
9	12.9	31.3	5.3	14.0	10.8	28.0
10	6.9	26.0	3.2	14.2	5.6	21.8
11	4.9	13.3	3.5	6.7	3.5	11.5
12	11.8	336.8	7.6	169.2	9.0	291.2

4. Discussion

Quality estimation of LRNTS is based on three criteria:

- (1) coverage of LRNTS navigation signals within the crater—viewsheds (Table 1 and Figure 6);

- (2) accuracy expressed as positional standard errors of the points (Table 2, Figures 7–9);
- (3) efficiency expressed as the number of points and measurements (Table 1).

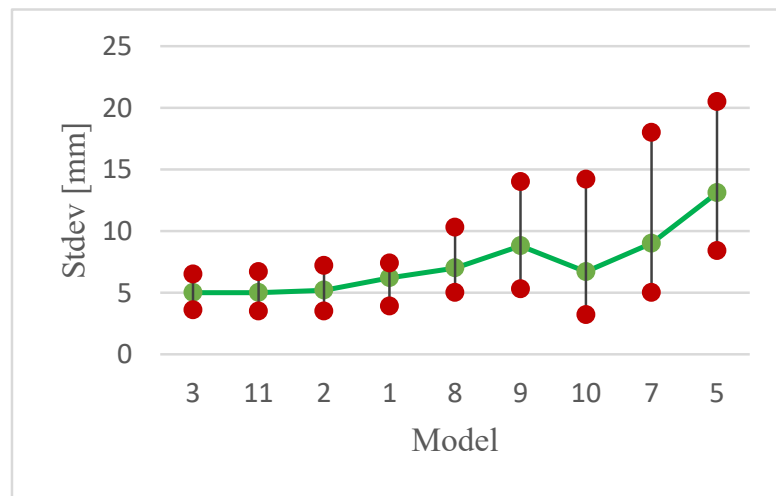


Figure 7. LRNTS horizontal standard deviations.

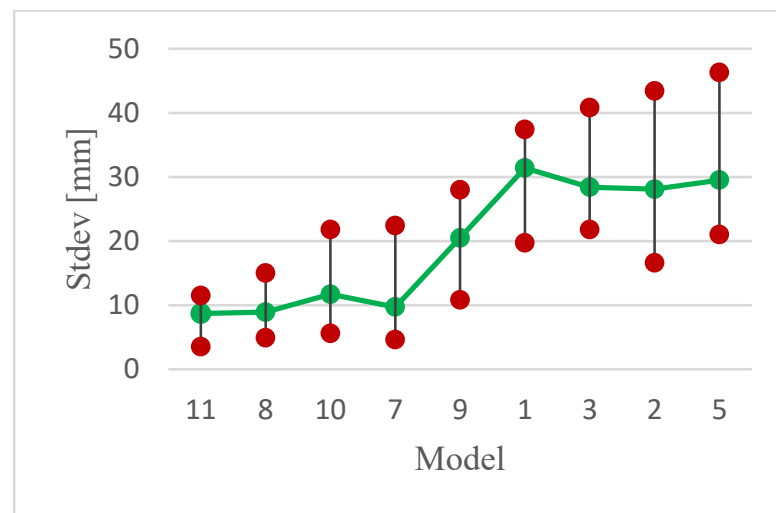


Figure 8. LRNTS vertical standard deviations.

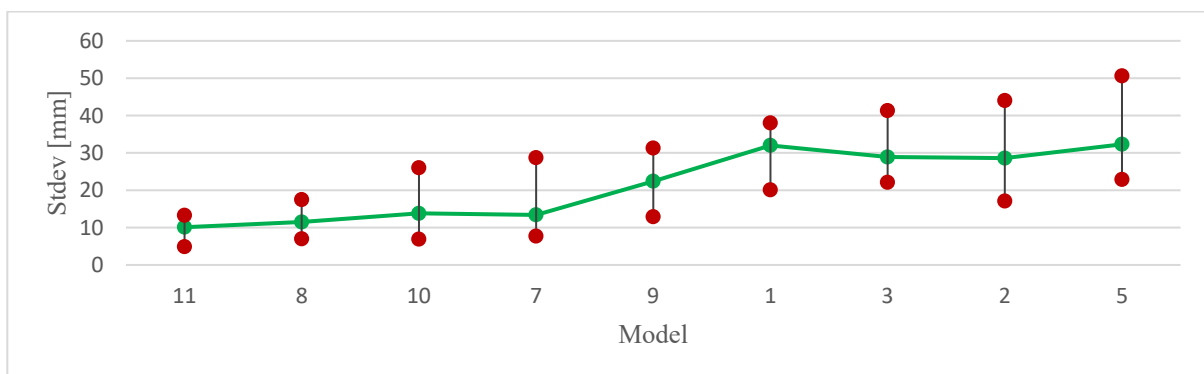


Figure 9. LRNTS spatial (3D) standard deviations.

Regarding the coverage of the crater area with transceiver signals, none of the configurations assure 100% signal availability within the crater. Table 1 displays the number of the transceivers in each configuration setup with the percentage of signal coverage within the crater. Among the 12 tested models, half of them (grey-shaded in Table 1) provide less than 95% signal availability, which limits their possible utilization.

Inspecting 3D position accuracies in Table 2, one can observe that the maximal standard deviations of the tested configuration setups are between 17.5 cm and 336.8 mm. Detailed analysis shows that the vertical component (z values) results in much larger standard deviations due to the adjustment linear model. Partial derivatives for the pseudo-distance P_{ij} (connecting transceivers i and j) over the unknown coordinate z_i of the design matrix A follow the form $\frac{\partial P_{ij}}{\partial z_i} = \frac{z_j - z_i}{D}$. Derivation over y_i and x_i gives analogue forms, replacing z with y and x , respectively. Since the transceiver height spans are smaller, in some cases, up to an order of value compared to horizontal components, the corresponding elements of A referring to the vertical component are proportionally smaller. Therefore, the cofactor matrix $Q_x = N^+ = (A^T P A)^{-1}$ produces elements related to the z coordinate much larger than for the x and y axes.

Bearing that in mind, the 3D problem is split into 2D + 1D. The calculated standard deviations of the horizontal positions and related vertical accuracies are given in columns 4–7 of Table 2. There are three models with extremely high standard deviations (shaded grey in Table 2). They are not taken into account with further processing. Graphical representations of the other nine models that fulfill the accuracy requirements, sorted with respect to their performance, are given in Figures 7–9.

The abscise holds the numbers of selected models (from Tables 1 and 2), while the results (minimum and maximum standard deviations) are given in mm and presented as short red vertical lines. The average standard deviation values for each model are connected with the green line.

Merging three criteria (viewsheds, accuracy, and the number of the transceivers), the optimal model is No. 11, with nine transceivers, a coverage of 95.5%, and maximal standard deviations of 6.7 mm for the horizontal position and 11.5 mm for the vertical component.

5. Conclusions

This paper suggests a new infrastructure for high-precision real-time positioning on the Moon, called the Lunar Regional Navigation Transceiver System. It is a ground system which transmits navigation messages similar to GNSS. The system itself is autonomous and capable of self-calibrating. It consists of a set of transceivers placed around the Lunar region where excavation or construction works are performed.

A case study presented here is implemented on the Shackleton Crater, which is a possible candidate for the first Lunar exploration works. A proof of a concept includes 12 different configuration setups for the transceivers' locations along the crater. All configurations were tested against accuracy, signal coverage (inter-visibility), and efficiency, in the sense of the number of the LRNTS nodes. Among 12 tested models, the setup consisting of nine nodes showed the best numerical figures, with horizontal accuracy of 6.7 mm and vertical accuracy of 11.5 mm and availability over 95.5% of the Shackleton area. If deployed in that way, such a reference frame allows centimeter-level real-time positioning of the user receivers throughout the crater. However, if millimeter-level accuracy is needed, local high-precision control networks can be developed around the desired construction spots in the same manner as in terrestrial applications. Then, the local control networks would be tied to the LRNTS coordinate system, including the points surveyed from the local network.

The results presented here can be replicated for other solar system bodies (preferably Mars) because the suggested methodology does not need permanent communication with the Earth, which makes the concept self-adjustable and self-sustainable. Practical implementation of this research could help all further missions aimed at Moon exploration, which will benefit from having a tested reliable system for precise positioning purposes during all construction and excavation works.

Author Contributions: Conceptualization, D.I.S.; methodology, D.I.S. and V.O.; software, V.O.; validation, J.R., V.P.-P. and G.V.; formal analysis, V.O.; investigation, D.I.S.; resources, D.I.S.; data curation, D.I.S. and V.O.; writing—original draft preparation, D.I.S. and V.O.; writing—review and editing, J.R., V.P.-P. and G.V.; visualization, D.I.S.; supervision, V.P.-P. and G.V.; project administration, V.P.-P. and G.V. All authors have read and agreed to the published version of the manuscript.

Funding: This research was funded by research program P2-0268 (ARRS Research and Infrastructure Programs) financed by the Slovenian Research Agency.

Data Availability Statement: All data used in this study are freely available on request to the authors.

Acknowledgments: This research was supported by the Slovenian Ministry of Education Science and Sport, Faculty of Natural Sciences and Engineering.

Conflicts of Interest: The authors declare no conflict of interest. The funders had no role in the design of the study; in the collection, analysis, or interpretation of data; in the writing of the manuscript; or in the decision to publish the results.

Abbreviations

The following abbreviations are used in this manuscript:

LRNTS	Lunar Regional Navigation Transceiver System
GNSS	Global Navigation Satellite System
ISRU	In Situ Resource Utilization
ISRO	Indian Space Research Organization
SLAM	Simultaneous Localization and Mapping
SINS	Strapdown Inertial Navigation System
QUEST	QUaternion ESTimator
SNE	Satellite Navigation Equipment
SCPA	Self-Calibrating Pseudolite Array
GPS	Global Navigation System
MMS	Magnetospheric Multiscale mission
GOES	Geostationary Operational Environmental Satellite
PSR	Permanently Shadowed Region
LRO	Lunar Reconnaissance Orbiter
SPA	South Pole Aitken
DEM	Digital Elevation Model
LLR	Lunar Laser Ranging
AFS	Atomic Frequency Standard
SIC	Successive Interference Calculation
STP	Space Time Processing

References

1. Hurst, C. China's Rare Earth Elements Industry: What Can the West Learn? Institute for the Analysis of Global Security (IAGS). 2010. Available online: https://www.researchgate.net/publication/235080237_China_T1\textquoterights_Rare_Earth_Elements_Industry_What_Can_the_West_Learn (accessed on 13 January 2023).
2. NASA. NASA's Lunar Exploration Program Overview. 2020. Available online: https://www.nasa.gov/sites/default/files/atoms/files/artemis_plan-20200921.pdf (accessed on 12 April 2022).
3. Shekhtman, L.; Thompson, J.R. Asteroids—NASA Solar System Exploration, NASA. 2019. Available online: https://solarsystem.nasa.gov/asteroids-comets-and-meteors/asteroids/overview/?page=0&per_page=40&order=name+asc&search=&condition_1=101%3Aparent_id&condition_2=asteroid%3Abody_type%3Alike (accessed on 14 January 2023).
4. ISECG. The Global Exploration Roadmap₂₀₂₂. 2022. Available online: https://www.globalspaceexploration.org/wp-content/isecg/GER_Supplement_Update_2022.pdf (accessed on 13 December 2022).
5. Pittman, R.B.; Harper, L.D.; Newfield, M.E.; Rasky, D.J. Lunar Station: The Next Logical Step in Space Development. *New Space* **2016**, *4*, 7–14. [CrossRef]
6. Goswami, N. India's space program, ambitions, and activities. *Asia Policy* **2020**, *15*, 43–49. [CrossRef]
7. ESA. ESA—Gateway with Orion Docked Right. 2019. Available online: https://www.esa.int/ESA_Multimedia/Images/2019/05/Gateway_with_Orion_docked_right (accessed on 15 April 2022).
8. ESA. Gateway to the Moon. 2019. Available online: https://www.esa.int/Science_Exploration/Human_and_Robotic_Exploration/Gateway_to_the_Moon (accessed on 15 April 2022).
9. Li, C.; Wang, C.; Wei, Y.; Lin, Y. China's present and future lunar exploration program. *Science* **2019**, *365*, 238–239. [CrossRef]

10. Clark, S. Russia Looks to China as New Space Exploration Partner. Spaceflight Now. 2021. Available online: <https://spaceflightnow.com/2021/03/15/russia-looks-to-china-as-new-space-exploration-partner/> (accessed on 12 April 2022).
11. Rio Tinto. What in the World Do Mining and Rocket Science Have in Common? 2019. Available online: <https://www.riotinto.com/en/news/stories/mining-rocket-science-common> (accessed on 6 May 2022).
12. Woods, B. Caterpillar and NASA Developing Autonomous Vehicles to Mine the Moon. CNBC. 2019. Available online: <https://www.cnbc.com/2019/10/23/caterpillar-and-nasa-developing-autonomous-vehicles-to-mine-the-moon.html> (accessed on 6 May 2022).
13. Stupar, D.I.; Ogrizović, V.; Rošer, J.; Vižintin, G. Analytical and Numerical Solution for Better Positioning in Mines with Potential Extending Application in Space Mining. *Minerals* **2022**, *12*, 640. [CrossRef]
14. Liu, J.; Ren, X.; Yan, W.; Li, C.; Zhang, H.; Jia, Y.; Zeng, X.; Chen, W.; Gao, X.; Liu, D.; et al. Descent trajectory reconstruction and landing site positioning of Chang'E-4 on the lunar farside. *Nat. Commun.* **2019**, *10*, 4229. [CrossRef]
15. Imbriale, W.A. *Large Antennas of the Deep Space Network*; Monograph 4 Deep—Space Communications and Navigation Series; JPL: Pasadena, CA, USA; NASA: Washington, DC, USA, 2002.
16. Bilodeau, V.S.; Clerc, S.; Drai, R.; de Lafontaine, J. Optical navigation system for pin-point lunar landing. In *IFAC Proceedings Volumes (IFAC-PapersOnline)*; IFAC: New York, NY, USA, 2014; pp. 10536–10542. [CrossRef]
17. Ma, Y.Q.; Liu, S.C.; Sima, B.; Wen, B.; Peng, S.; Jia, Y. A precise visual localisation method for the Chinese Chang'e-4 Yutu-2 rover. *Photogramm. Rec.* **2020**, *35*, 10–39. [CrossRef]
18. Schönfeldt, M.; Grenier, A.; Delépaut, A.; Swinden, R.; Giordano, P.; Ventura-Traveset, J. Across the Lunar Landscape—Exploration with GNSS Technology—Inside GNSS—Global Navigation Satellite Systems Engineering. Policy, and Design, Inside GNSS. 2020. Available online: <https://insidegnss.com/across-the-lunar-landscape-exploration-with-gnss-technology/> (accessed on 6 May 2022).
19. Guan, X.; Wang, X.; Fang, J.; Feng, S. An innovative high accuracy autonomous navigation method for the Mars rovers. *Acta Astronaut.* **2014**, *104*, 266–275. [CrossRef]
20. Xu, F.; Fang, J. Velocity and position error compensation using strapdown inertial navigation system/celestial navigation system integration based on ensemble neural network. *Aerosp. Sci. Technol.* **2008**, *12*, 302–307. [CrossRef]
21. Wei, X.; Cui, C.; Wang, G.; Wan, X. Autonomous positioning utilizing star sensor and inclinometer. *Measurement* **2019**, *131*, 132–142. [CrossRef]
22. Hamera, K.E.; Mosher, T.; Gefreh, M.; Paul, R.; Slavkin, L.; Trojan, J. An evolvable lunar communication and navigation constellation architecture. In Proceedings of the 26th AIAA International Communications Satellite Systems Conference ICSSC, San Diego, CA, USA, 10–12 June 2008.
23. Delépaut, A.; Giordano, P.; Ventura-Traveset, J.; Blonski, D.; Schönfeldt, M.; Schoonejans, P.; Aziz, S.; Walker, R. Use of GNSS for lunar missions and plans for lunar in-orbit development. *Adv. Space Res.* **2020**, *66*, 2739–2756. [CrossRef]
24. Mikrin, E.A.; Mikhailov, M.V.; Orlovskii, I.V.; Rozhkov, S.N.; Krasnopol'skii, I.A. Satellite Navigation of Lunar Orbiting Spacecraft and Objects on the Lunar Surface. *Gyroscopy Navig.* **2019**, *10*, 54–61. [CrossRef]
25. LeMaster, E.A. Self Calibrating Pseudolite Arrays—Theory and Experiment. Master's Thesis, Stanford University, Stanford CA, USA, 2002. Available online: <https://web.stanford.edu/group/arl/cgi-bin/drupal/sites/default/files/public/publications/LeMaster%202002.pdf> (accessed on 27 February 2023).
26. Lemaster, E.A.; Rock, S.M. A Local-Area GPS Pseudolite-Based Mars Navigation System. In Proceedings of the IEEE 10th International Conference on Advanced Robotics, Budapest, Hungary, 22–25 August 2001.
27. Stone, J.M.; LeMaster, E.A.; David Powell, J.; Rock, S. GPS Pseudolite Transceivers and their Applications. In Proceedings of the 1999 National Technical Meeting of the Institute of Navigation, San Diego, CA, USA, 25–27 January 1999.
28. Cobb, H.S. GPS Pseudolites: Theory, Design, and Applications. 1997. Available online: <https://web.stanford.edu/group/scpnt/gpslab/pubs/theses/StewartCobbThesis97.pdf> (accessed on 26 February 2023).
29. Jenner, L. NASA Eyes GPS at the Moon for Artemis Missions. NASA Space Technology. 2019. Available online: <http://www.nasa.gov/feature/goddard/2019/nasa-eyes-gps-at-the-moon-for-artemis-missions> (accessed on 1 May 2022).
30. HAKUTO-R Mission 1 | ispace. Available online: <https://ispace-inc.com/m1> (accessed on 17 January 2023).
31. NASA: Artemis, I. Available online: <https://www.nasa.gov/specials/artemis-i/> (accessed on 26 February 2023).
32. ESA—Moonlight. Available online: https://www.esa.int/Applications/Telecommunications_Integrated_Applications/Moonlight (accessed on 26 February 2023).
33. Baird, D. NASA Mirrors on ESA Pathfinder to Enhance Lunar Navigation. 2022. Available online: <http://www.nasa.gov/feature/goddard/2022/nasa-mirrors-on-esa-pathfinder-to-enhance-lunar-navigation> (accessed on 26 February 2023).
34. CSEM. *The Scientific Context for Exploration of the Moon*; National Academies Press: Washington, DC, USA, 2007. [CrossRef]
35. Mitchell, J.; Lawrence, S.; Robinson, M.; Speyerer, E.; Denevi, B. Using complementary remote sensing techniques to assess the presence of volatiles at the lunar north pole. *Planet. Space Sci.* **2018**, *162*, 133–147. [CrossRef]
36. Mazarico, E.; Neumann, G.A.; Smith, D.E.; Zuber, M.T.; Torrence, M.H. Illumination conditions of the lunar polar regions using LOLA topography. *Icarus* **2011**, *211*, 1066–1081. [CrossRef]
37. Bussey, D.B.J.; Spudis, P.D.; Robinson, M.S. Illumination conditions at the lunar South Pole. *Geophys. Res. Lett.* **1999**, *26*, 1187–1190. [CrossRef]
38. Wingo, D. Site Selection for Lunar Industrialization, Economic Development, and Settlement. *New Space* **2016**, *4*, 19–39. [CrossRef]

39. Zuber, M.T.; Head, J.W.; Smith, D.E.; Neumann, G.A.; Mazarico, E.; Torrence, M.H.; Aharonson, O.; Tye, A.R.; Fassett, C.I.; Rosenburg, M.A.; et al. Constraints on the volatile distribution within Shackleton crater at the lunar south pole. *Nature* **2012**, *486*, 378–381. [[CrossRef](#)]
40. Vanoutryve, B.; de Rosa, D.; Fisackerly, R.; Houdou, B.; Carpenter, J.; Philippe, C.; Pradier, A.; Jojaghalian, A.; Espinasse, S.; Gardini, B. *An Analasys of Illumination and Communication Conditions near Lunar South Pole Based on Kaguya Data*; ESA: Paris, France, 2010.
41. Barker, M.K.; Mazarico, E.; Neumann, G.A.; Zuber, M.T.; Haruyama, J.; Smith, D.E. A new lunar digital elevation model from the Lunar Orbiter Laser Altimeter and SELENE Terrain Camera. *Icarus* **2016**, *273*, 346–355. [[CrossRef](#)]
42. Kokhanov, A.A.; Karachevtseva, I.P.; Zubarev, A.E.; Patraty, V.; Rodionova, Z.F.; Oberst, J. Mapping of potential lunar landing areas using LRO and SELENE data. *Planet. Space Sci.* **2017**, *162*, 179–189. [[CrossRef](#)]
43. Basilevsky, A.T.; Krasilnikov, S.S.; Ivanov, M.A.; Malenkov, M.I.; Michael, G.G.; Liu, T.; Head, J.W.; Scott, D.R.; Lark, L. Potential Lunar Base on Mons Malapert: Topographic, Geologic and Trafficability Considerations. *Sol. Syst. Res.* **2019**, *53*, 383–398. [[CrossRef](#)]
44. Mahoney, E. (Ed.) *The Global Exploration Roadmap Supplement Octobar*; NASA: Washington, DC, USA, 2022. Available online: https://www.nasa.gov/sites/default/files/atoms/files/ger-supplement-update-2022-final-10-6-22_tagged.pdf (accessed on 11 December 2022).
45. Ludivig, P.; Olivares-mendez, M.; Diaz, A.C.; Ivanov, D.; Voos, H.; Lamamy, J. Testing Environments for Lunar Surface Perception Systems; Combining Indoor Facilities, Virtual Environments and Analogue Field Tests. In Proceedings of the I-SAIRAS 2020, Pasadena, CA, USA, 19–23 October 2020.
46. Sherwood, B. Principles for a practical Moon base. *Acta Astronaut.* **2019**, *160*, 116–124. [[CrossRef](#)]
47. Powering the Moon: Designing a Microgrid for Future Lunar Base. 2022. Available online: <https://phys.org/news/2022-05-powering-moon-microgrid-future-lunar-1.html> (accessed on 11 December 2022).
48. LOLA, S.T. Moon LRO LOLA DEM 118m v1 | USGS Astrogeology Science Center. 2014. Available online: https://astrogeology.usgs.gov/search/details/Moon/LRO/LOLA/Lunar_LRO_LOLA_Global_LDEM_118m_Mar2014/cub (accessed on 6 May 2021).
49. Williams, J.G.; Boggs, D.H.; Folkner, W.M. *DE430 Lunar Orbit, Physical Librations, and Surface Coordinates*; Jet Propulsion Laboratory: Pasadena, CA, USA, 2013; pp. 1–19. [[CrossRef](#)]
50. Folkner, W.M.; Williams, J.G.; Boggs, D.H.; Park, R.S.; Kuchynka, P. The Planetary and Lunar Ephemerides DE430 and DE431. *Interplanet. Netw. Prog. Rep.* **2014**, *196*, 42–196.
51. Chowdhury, D.D. *NextGen Network Synchronization*; Springer: Berlin/Heidelberg, Germany, 2021. [[CrossRef](#)]
52. Martinez, F.J.G. *Performance of New GNSS Satellite Clocks*; KIT Scientific Publishing: Karlsruhe, Germany, 2014. [[CrossRef](#)]
53. Madhani, P.H.; Axelrad, P.; Krumvieda, K.; Thomas, J. Application of successive interference cancellation to the GPS pseudolite near-far problem. *IEEE Trans. Aerosp. Electron. Syst.* **2003**, *39*, 481–488. [[CrossRef](#)]
54. Martin, S.; Kuhlen, H.; Abt, T. Interference and regulatory aspects of GNSS pseudolites. In Proceedings of the 18th International Technical Meeting of the Satellite Division of the Institute of Navigation, ION GNSS 2005, Long Beach, CA, USA, 13–16 September 2005. [[CrossRef](#)]
55. Chang, C.L.; Juang, J.C. Performance analysis of narrowband interference mitigation and near-far resistance scheme for GNSS receivers. *Signal Process.* **2010**, *90*, 2676–2685. [[CrossRef](#)]
56. Marathe, T.; Daneshmand, S.; Lachapelle, G. Pseudolite interference mitigation and signal enhancements using an antenna array. In Proceedings of the 2015 International Conference on Indoor Positioning and Indoor Navigation, IPIN 2015, Banff, AB, Canada, 13–16 October 2015. [[CrossRef](#)]
57. Zheng, Z.H.; Wang, B.; Zhou, Z.Q.; Gao, Z.F. A scene matching method for automatic and precise soft landing on the lunar surface. *Beijing Ligong Daxue Xuebao/Trans. Beijing Inst. Technol.* **2013**, *33*, 172–177.
58. Remesh, N.; Ramanan, R.V.; Lalithambika, V.R. A Novel Indirect Scheme for Optimal Lunar Soft Landing at a Target Site. *J. Inst. Eng. Ser. C* **2021**, *102*, 1379–1393. [[CrossRef](#)]
59. Hu, T.; He, L.; Cao, T.; Zhang, H.; Hu, Y.; Qian, Z. Autonomous Obstacle Detection and Avoidance of Lunar Landing Based on Active and Passive Sensors. In Proceedings of the 2021 International Symposium on Computer Science and Intelligent Controls, ISCSIC 2021, Rome, Italy, 12–14 November 2021. [[CrossRef](#)]
60. Wong, U.H.; Wu, Y.; Wong, H.C.; Liang, Y.; Tang, Z. Modeling the reflectance of the lunar regolith by a new method combining Monte Carlo ray tracing and Hapke’s model with application to chang’e-1 IIM data. *Sci. World J.* **2014**, *2014*, 457138. [[CrossRef](#)] [[PubMed](#)]
61. Petrova, E.V.; Markiewicz, W.J.; Keller, H.U. Regolith Surface Reflectance: A New Attempt to Model. *Sol. Syst. Res.* **2001**, *35*, 278–290. [[CrossRef](#)]
62. Heiken, G.H.; Vaniman, D.T.; French, B.M. *Lunar Sourcebook: A User’s Guide to the Moon*; Cambridge University Press: Cambridge, UK, 1991.
63. Gaier, J.R. The Effects of Lunar Dust on EVA Systems during the Apollo Missions. 2005. Available online: <http://www.sti.nasa.gov> (accessed on 11 December 2022).
64. Budzyń, D.; Zare-Behtash, H.; Cowley, A.; Cammarano, A. Implicit lunar dust mitigation technology: Compliant mechanisms. *Acta Astronaut.* **2023**, *203*, 146–156. [[CrossRef](#)]

65. Budzyń, D.; Tuohy, E.; Garrivier, N.; Schild, T.; Cowley, A.; Cruise, R.; Adachi, M.; Zare-Behtash, H.; Cammarano, A. Lunar Dust: Its Impact on Hardware and Mitigation Technologies. In Proceedings of the 46th Aerospace Mechanisms Symposium, Houston, TX, USA, 11–13 May 2022.
66. Climent, B.; Torroba, O.; González-Cinca, R.; Ramachandran, N.; Griffin, M.D. Heat storage and electricity generation in the Moon during the lunar night. *Acta Astronaut.* **2014**, *93*, 352–358. [[CrossRef](#)]
67. Ulamec, S.; Biele, J.; Trollope, E. How to survive a Lunar night. *Planet. Space Sci.* **2010**, *58*, 1985–1995. [[CrossRef](#)]
68. Hofmann-Wellenhof, E.; Lichtenegger, B.; Wasle, H. Observables. In *GNSS—Global Navigation Satellite Systems*; Springer Vienna: Vienna, Austria, 2007; pp. 105–160. [[CrossRef](#)]

Disclaimer/Publisher’s Note: The statements, opinions and data contained in all publications are solely those of the individual author(s) and contributor(s) and not of MDPI and/or the editor(s). MDPI and/or the editor(s) disclaim responsibility for any injury to people or property resulting from any ideas, methods, instructions or products referred to in the content.